Lateral stability of imperfect discretely-braced steel beams

Finian McCann,* M. Ahmer Wadee† and Leroy Gardner‡

April 3, 2013

Abstract

The lateral stability of imperfect discretely-braced steel beams is analyzed using Rayleigh–Ritz approximations for the lateral deflection and the angle of twist. Initially, it is assumed that these degrees-of-freedom can be represented by functions comprising only single harmonics; this is then compared to the more accurate representation of the displacement functions by full Fourier series. It is confirmed by linear eigenvalue analysis that the beam can realistically buckle into two separate classes of modes: a finite number of node-displacing modes, equal to the number of restraints provided, and an infinite number of single harmonic buckling modes where the restraint nodes remain undeflected. Closed-form analytical relations are derived for the elastic critical moment of the beam, the forces induced in the restraints and the minimum stiffness required to enforce the first internodal buckling mode. The position of the restraint above or below the shear center is shown to influence the overall buckling behavior of the beam. The analytical results for the critical moment of the beam are validated by the finite element program LTBeam, while the results for the deflected shape of the beam are validated by the numerical continuation software AUTO-07p, with very close agreement between the analytical and numerical results.

*Doctoral student, Department of Civil and Environmental Engineering, Imperial College London, London SW7 2AZ, UK

†Reader in Nonlinear Mechanics, Department of Civil and Environmental Engineering, Imperial College London, London SW7 2AZ, UK

‡Reader in Structural Engineering, Department of Civil and Environmental Engineering, Imperial College London, London SW7 2AZ, UK

1 Introduction

Slender beams are susceptible to failure through lateral-torsional buckling, an instability phenomenon involving both lateral deflection and twist of the cross-section of the beam. The stability of a beam can be enhanced through the provision of restraints that inhibit either one, or both, of these forms of displacement, thus increasing the overall load that the beam can safely support. Restraints can be continuous, like profiled metal sheeting, or discrete, like roof purlins. If they inhibit the amount of twist at a particular cross-section then they are described as torsional restraints; if they inhibit the lateral deflection of the section, they are described as lateral restraints. The current work focuses on beams with discrete lateral restraints.

The classical result for the critical lateral-torsional buckling moment of a beam simply-supported in and out of plane without intermediate restraint under constant bending moment, as given by Timoshenko & Gere (1961), is:

$$M_{\mathrm{ob}} = \frac{\pi^2 E I_z}{L^2}\sqrt{\frac{I_w}{I_z} + \frac{L^2 G I_t}{\pi^2 E I_w}}, \tag{1}$$

where the material properties E and G are the Young's modulus and elastic shear modulus, respectively, of steel; the cross-sectional properties I_z, I_w and I_t are the minor-axis second moment of area, the warping stiffness and the St. Venant's torsional constant, respectively.

Flint (1951) was the first to examine analytically the beneficial effect of providing beams with lateral restraints, making use of variational methods to derive expressions for the critical moment of a beam with a single central elastic restraint. A limiting restraint stiffness was found at which the beam would buckle without displacing the restraint node, in contrast with the node-displacing buckling shape that occurred for less stiff restraints. Subsequent work by Zuk (1956), Winter (1960) and Taylor & Ojalvo (1966) expanded on the work of Flint to examine forces transmitted to the restraints and the influence of various types of restraint. In these works, it was again assumed that the buckling shape was a single harmonic wave; it is shown in the current work that such an assumption leads to erroneous predictions of key features such as critical moment, required brace stiffness and displaced shape. Finite element analyses, such as those performed by Nethercot & Rockey (1971) and Mutton & Trahair (1973), circumvented such assumptions, providing more accurate results for the critical moment and the required brace stiffness.

Trahair & Nethercot (1984) presented specific results for beam-columns with continuous restraint and outlined how the stiffness matrix could be adapted for discrete braces. The critical moment of a beam with multiple discrete rigid (infinitely stiff) lateral braces was provided; for elastic restraints, the work of Medland (1980) was referenced, but no explicit expressions were given. Trahair (1993) suggested to represent the system of braces as an equivalent continuous restraint of stiffness, a procedure referred to currently as smearing; this is also shown in the current work to lead to erroneous predictions.

Yura (2001) confirmed that compression flange braces are the most efficient and that when web distortion was accounted for, there was a loss of efficiency for braces positioned at the shear center. It is assumed in the current work that webs are adequately stiffened at bracing nodes.

Thus, it is the aim of the current work to determine key features of a laterally-braced beam system by analytical, rather than numerical, means, for an arbitrary number of restraints positioned at an arbitrary height above the shear center.

2 Model under investigation

The model under investigation (see Figure 1) is that of a simply-supported doubly-symmetric I-beam of span L with n_b discrete linearly elastic restraints located regularly along the span, so that the restraint spacing $s = L/(n_b + 1)$. Equal but opposite end moments create a constant bending moment of magnitude M throughout the beam. The restraints are linearly elastic and each one is of stiffness K. They are positioned at a height a above the shear center, with $a > 0$ denoting compression side restraints. The rigid cross-section condition of Vlasov (1961) is assumed and so there are two degrees-of-freedom: the lateral deflection of the shear center of the cross-section of the beam, u, and the angle of twist of the cross-section about the longitudinal x axis, ϕ.

An expression for the total potential energy, V, of the system is obtained by modifying that of Pi *et al.* (1992), which is linearized by assuming small deflections, to include the strain energy stored in the restraints and also to include the effects of an initial lateral imperfection e by applying the concept of a strain-relieved initial configuration of Thompson & Hunt (1984). The resulting expression, with primes denoting differentiation with respect to the longitudinal coordinate x, is:

$$V = \int_0^L \frac{1}{2}\left[EI_z(u''-e'')^2 + EI_w\phi''^2 + GI_t\phi'^2 + 2Mu''\phi\right]\mathrm{d}x + \frac{1}{2}K\sum_{i=1}^{n_b} X_i^2, \tag{2}$$

where X_i is the extension of the ith restraint located at $x = iL/(n_b+1)$ and:

$$X(x) = u(x) + a\phi(x) - e(x). \tag{3}$$

3 Single harmonic representation

3.1 Potential energy

As a simplistic assumption of the buckled shape of a beam, the displacement functions u and ϕ are defined thus:

$$\frac{u}{u_n} = \frac{\phi}{\phi_n} = \sin\left(\frac{n\pi x}{L}\right), \tag{4}$$

where u_n and ϕ_n are the maximum amplitudes of u and ϕ, respectively and are the generalized coordinates of the system; in the current section, only critical equilibrium is of interest and so the form of the imperfection may be ignored.

3.1.1 Node-displacing harmonics

Harmonic numbers n where $n \bmod (n_b+1) \neq 0$, are termed node-displacing harmonics. Owing to the orthogonality of the sine function, upon integration, V reduces to:

$$V = \frac{L}{4}\left[EI_z\left(\frac{n\pi}{L}\right)^4(u_n-e)^2 + EI_w\left(\frac{n\pi}{L}\right)^4\phi_n^2 + GI_t\left(\frac{n\pi}{L}\right)^2\phi^2 - 2M\left(\frac{n\pi}{L}\right)^2u_n\phi_n\right] \tag{5}$$

$$+\frac{1}{2}K\left(\frac{n_b+1}{2}\right)(u_n + a\phi_n - e_n)^2,$$

since periodic functions in the restraint energy term outside the integral are replaced by:

$$\sum_{i=1}^{n_b} \sin^2\left(\frac{in\pi}{n_b+1}\right) = \frac{n_b+1}{2}, \tag{6}$$

a relationship that can be proven using difference calculus (McCann, 2012).

3.1.2 Internodal harmonics

For $n \bmod (n_b+1) = 0$, termed internodal harmonics, the restraint spacing s is an integer multiple of the wavelength of the harmonic displacement function and thus there is no displacement of the restraint nodes. This, in turn, implies that there is no strain energy stored in the restraints. The associated total potential energy, V_i, reduces to:

$$V_i = \frac{L}{4}\left[EI_z\left(\frac{n\pi}{L}\right)^4 (u_n - e)^2 + EI_w\left(\frac{n\pi}{L}\right)^4 \phi_n^2 + GI_t\left(\frac{n\pi}{L}\right)^2 \phi^2 - 2M\left(\frac{n\pi}{L}\right)^2 u_n\phi_n\right]. \tag{7}$$

3.2 Linear eigenvalue analysis

The critical moment of the system is found by solving $\det(\mathbf{H}) = 0$ for M, where $\mathbf{H}$ is the Hessian matrix of the system, *i.e.* the matrix of second derivatives of V (or V_i for internodal harmonics) with respect to the generalized coordinates; it is assumed for the linear eigenvalue analysis that $e = 0$. For internodal harmonic numbers of the form $q(n_b+1)$, the nondimensional critical moment is:

$$\hat{M}_{\mathrm{cr},q(n_b+1)} = q^2(n_b+1)^2\sqrt{1+\frac{\kappa}{q^2\left(n_b+1\right)^2}}, \tag{8}$$

where $q \in \mathbb{N}$ and $\hat{M} = 2M/P_E h_s$, $P_E = \pi^2 EI_z/L^2$, $\kappa = L^2 GI_t/\pi^2 EI_w$ and $I_w = I_z h_s^2/4$ for I-sections, and h_s is the depth between the shear centers of the flanges. The lowest possible internodal critical moment of course occurs for $q = 1$; this value of the critical moment is known as the threshold moment, M_T, and corresponds to a beam buckling in between the restraint nodes *i.e.* when the harmonic number $n = n_b + 1$:

$$\hat{M}_T = (n_b+1)^2\sqrt{1+\frac{\kappa}{\left(n_b+1\right)^2}}. \tag{9}$$

For node-displacing harmonics, the nondimensional critical moment, found by solving $\det(\mathbf{H}) = 0$ for the expression of V in Equation (5), is given by:

$$\hat{M}_{\mathrm{cr},n} = \sqrt{\left[n^2 + \left(\frac{n_b+1}{n^2}\right)\gamma\right]\left[n^2 + \kappa + \hat{a}^2\left(\frac{n_b+1}{n^2}\right)\gamma\right]} + \hat{a}\left(\frac{n_b+1}{n^2}\right)\gamma, \qquad (10)$$

where $\gamma = KL/\pi^2 P_E$ and $\hat{a} = 2a/h_s$. The value of the critical moment for node-displacing modes is clearly dependent upon the magnitude of the restraint stiffness, and increases as the restraint stiffness is increased. For $K = 0$, *i.e.* an unrestrained beam, $M_{\mathrm{cr},n+1} > M_{\mathrm{cr},n}$; however, as shown in Figure 2, once a relevant transition stiffness is exceeded, $M_{\mathrm{cr},n+1} < M_{\mathrm{cr},n}$, and the mode corresponding to the higher harmonic is now in fact the critical mode. At a certain threshold stiffness, K_T, all the critical moments associated with the node-displacing modes exceed the threshold moment, and the internodal buckling mode is the critical mode; this level of restraint is referred to as "full bracing". Since full bracing corresponds to a buckled shape with a harmonic number n_b+1, there can be a maximum of n_b possible critical node-displacing modes for $K < K_T$; however, this does not necessarily imply that the mode number n_T at which the transition from node-displacing to internodal buckling occurs is necessarily equal to n_b. The nondimensional threshold stiffness $\gamma_{T,n}$ corresponding to the nth node-displacing mode is found by equating $\hat{M}_{\mathrm{cr},n}$ with $\hat{M}_T$ and solving for γ:

$$\gamma_{T,n} = \left(\frac{n^2}{n_b+1}\right)\frac{\left[(n_b+1)^2 - n^2\right]\left[(n_b+1)^2 + n^2 + \kappa\right]}{n^2(1+\hat{a}^2) + \kappa + 2\hat{a}(n_b+1)^2\sqrt{1+\frac{\kappa}{(n_b+1)^2}}}. \qquad (11)$$

In a manner analogous to obtaining the critical buckling mode for a given restraint stiffness, by identifying the mode with the smallest corresponding critical moment, the mode at which the buckling behavior changes from node-displacing to internodal is that with the largest corresponding threshold stiffness, *i.e.* the maximum value of $\gamma_{T,n}$. Solving $\mathrm{d}\gamma_{T,n}/\mathrm{d}n = 0$ for n shows that $n_T < n_b + 1$; in fact, the maximum value of the $\gamma_{T,n}$ function can be shown to be located at $n = (n_b+1)/\sqrt{2}$ (McCann, 2012). Depending on the combination of beam geometry and restraint position, the actual maximum value can be somewhat lower than this. Since the actual value of n_T must be an integer, for $n_b \leqslant 3$, $n_T = n_b$; however, for $n_b \geqslant 4$, $n_T < n_b$ and there is mode-skipping since a full sequential progression of critical modes from $n = 1$ to n_b cannot be predicted when representing the displacement functions as single harmonics (see Figure 3). The implication of this is that there does not exist a general rule for determining the node-displacing mode at which the switch to internodal buckling occurs; instead, different values of n must be trialled to ensure that the correct mode, and consequently the correct threshold stiffness, is determined.

4 Fourier series representation

4.1 Mode separation

The displacement functions, u and ϕ, and the initial lateral imperfection, e, are now modelled as Fourier sine series. Any arbitrary initial imperfection can be specified by setting the values of e_n appropriately. The coefficients of the cosine terms are set equal to zero to satisfy the boundary conditions of zero displacement and zero twist at the supports:

$$u = \sum_{n=1}^{\infty} u_n \sin\left(\frac{n\pi x}{L}\right), \tag{12}$$

$$\phi = \sum_{n=1}^{\infty} \phi_n \sin\left(\frac{n\pi x}{L}\right), \tag{13}$$

$$e = \sum_{n=1}^{\infty} e_n \sin\left(\frac{n\pi x}{L}\right). \tag{14}$$

Upon substitution of each series into Equation (2), the total potential energy of the system is given by:

$$\begin{aligned} V = \int_0^L \frac{1}{2}\sum_{n=1}^{\infty}\sum_{m=1}^{\infty} \Bigg[& EI_z\left(\frac{n^2m^2\pi^4}{L^4}\right)(u_n - e_n)(u_m - e_m) + EI_w\left(\frac{n^2m^2\pi^4}{L^4}\right)\phi_n\phi_m \\ & + GI_t\left(\frac{nm\pi^2}{L^2}\right)\phi_n\phi_m - 2M\left(\frac{n^2\pi^2}{L^2}\right)u_n\phi_m\Bigg] \sin\left(\frac{n\pi x}{L}\right)\sin\left(\frac{m\pi x}{L}\right)\,\mathrm{d}x \\ & + \frac{1}{2}K\sum_{i=1}^{n_b}\sum_{n=1}^{\infty}\sum_{m=1}^{\infty}(u_n + a\phi_n - e_n)(u_m + a\phi_m - e_m)\sin\left(\frac{in\pi}{n_b+1}\right)\sin\left(\frac{im\pi}{n_b+1}\right). \end{aligned} \tag{15}$$

Upon evaluation of the integral, terms containing $\sin(n\pi x/L)\sin(m\pi x/L)$ where $n \neq m$ vanish due to the orthogonality of the sine function. However, this does not occur for terms outside the integral, *i.e.* in the restraint strain energy term; instead, there is interaction between harmonics with numbers n and m that obey $(n \pm m) \bmod 2(n_b+1) = 0$, while all other terms vanish, since:

$$\sum_{i=1}^{n_b} \sin\left(\frac{in\pi}{n_b+1}\right) \sin\left(\frac{im\pi}{n_b+1}\right) = 0\,\forall\,(n \pm m) \bmod 2(n_b+1) \neq 0, \tag{16}$$

a relationship that can be proven using difference calculus (McCann, 2012). Thus, the following potential energy functional is obtained:

$$V = \frac{L}{4}\sum_{n=1}^{\infty}\left[EI_z\left(\frac{n\pi}{L}\right)^4(u_n-e_n)^2 + EI_w\left(\frac{n\pi}{L}\right)^4\phi_n^2 + GI_t\left(\frac{n\pi}{L}\right)^2\phi_n^2 - 2M\left(\frac{n\pi}{L}\right)^2 u_n\phi_n\right]$$

$$+\frac{n_b+1}{4}K\sum_{n=1}^{\infty}\sum_{m\in H_n}\delta_{n,m}(u_n+a\phi_n-e_n)(u_m+a\phi_m-e_m)\,. \tag{17}$$

The sign operator function, $\delta_{n,m} = \pm 1$ if $(n \mp m) \bmod 2(n_b+1) = 0$ (otherwise $\delta_{n,m} = 0$). The set H_n is the set of harmonic numbers m that interact in the manner described above with n, or $H_n = \{m : (n \pm m) \bmod 2(n_b+1) = 0, m > 0\}$; the modularity involved in this definition makes it sufficient to define n_b different sets of interacting harmonics, *i.e.* $H_1, H_2, ..., H_{n_b}$. A crucial point to note is that the elements of each of these sets are uniquely their own, *i.e.* $H_i \cap H_j = \emptyset$.

Since the coordinates separate into distinct sets, the linear system of equations represented by the Hessian matrix $\mathbf{H}$ separates into distinct separate systems: a finite number n_b of modes that each relate to a particular harmonic set H_n, and an infinite number of modes relating to harmonic numbers of the form $q(n_b+1)$, which are not included in any set H_n. These two different classes of deflection modes are node-displacing and internodal modes, respectively, and are analogous to those mentioned in the previous section concerning single harmonic representations of the displacement functions.

4.2 Deflected shape and restraint forces

For the mth node-displacing mode, a system of linear equilibrium equations in u_n and ϕ_n is constructed from $\partial V/\partial u_n = 0$ and $\partial V/\partial \phi_n = 0$; of course, since only one particular mode is being considered, not all harmonics are involved and so a wave number $w_{i,j}$ is defined whereby, if the elements of H_i are ordered by increasing magnitude, then $w_{i,j}$ is the jth element of H_i. Simultaneous solution of the system of equations for all values of $u_{w_{m,n}}$ and $\phi_{w_{m,n}}$ leads to the following closed-form expressions for the harmonic amplitudes in terms of the imperfection amplitudes:

$$u_{w_{m,n}} = \frac{B_n + \hat{M}^2}{B_n} e_{w_{m,n}} + \frac{(-1)^n \hat{M} A_n}{w_{m,n}^2 B_n} \frac{S_1}{\frac{1}{(n_b+1)\gamma} + S_2}\,, \tag{18}$$

$$\phi_{w_{m,n}} = \frac{2}{h_s} \left[\frac{w_{m,n}^2 \hat{M}}{B_n} e_{w_{m,n}} + \frac{(-1)^n \hat{M}(w_{m,n}^2 \hat{a} + \hat{M})}{w_{m,n}^2 B_n} \frac{S_1}{\frac{1}{(n_b+1)\gamma} + S_2} \right], \tag{19}$$

where:

$$S_1 = \sum_i^{\infty} (-1)^{i+1} \frac{w_{m,i}^2 \hat{a} + \hat{M}}{B_i} e_{w_{m,i}}, \tag{20}$$

$$S_2 = \sum_i^{\infty} \frac{C_i}{w_{m,i}^2 B_i}, \tag{21}$$

$$A_n = w_{m,n}^2 + \kappa + \hat{a}\hat{M}, \tag{22}$$

$$B_n = w_{m,n}^4 + w_{m,n}^2 \kappa - \hat{M}^2, \tag{23}$$

$$C_n = w_{m,n}^2 (1 + \hat{a}^2) + \kappa + 2\hat{a}\hat{M}. \tag{24}$$

Now, considering the contribution of all the node-displacing deflection modes, an expression for the force induced in the ith restraint, F_i, as a proportion of the maximum compressive force in the beam, $P = M/h_s$, can be obtained by substituting Equations (18) and (19) into Equation (3), and noting that the restraints are linearly elastic, $F_i = KX_i$, the ratio F_I/P is obtained:

$$\frac{F_i}{P} = \frac{2\pi^2\gamma}{L} \sum_{m=1}^{n_b} \frac{S_1}{1 + (n_b+1)\gamma S_2} \sin \frac{im\pi}{n_b + 1}\,. \tag{25}$$

If the mth mode is isolated, it can be seen that the deflected positions of the restraint nodes follow a locus of m half-sine waves. If it is assumed that the imperfection is in the form of a single half-sine wave, as also assumed by Steel Construction Institute (2009), Al-Shawi (2001) and Trahair *et al.* (2008), *i.e.* $e = e_1 \sin(\pi x/L)$, then for all node-displacing modes other than the first, the theory does not predict any pre-buckling deflections, and likewise for the internodal modes. The expression for the restraint force ratio F_i/P becomes:

$$\frac{F_i}{P} = 2\pi^2\gamma \sin \frac{i\pi}{n_b + 1} \left(\frac{\hat{a} + \hat{M}}{1 + \kappa - \hat{M}^2} \right) \left(\frac{1}{1 + (n_b+1)\gamma S_2} \right) \frac{e_1}{L}. \tag{26}$$

4.3 Critical moment

An implicit load–deflection relationship can be inferred from Equations (18) and (19). Since the system is linear, a state of critical equilibrium is associated with a hypothetical deflection of arbitrary magnitude and a fixed critical load (or, in the current case, moment) and so the equilibrium path approaches a flat critical state asymptotically. Thus, conversely, a solution for the critical moment of the system can be obtained by determining the asymptote of a graph of u_n against $\hat{M}$; this relationship is independent of the initial imperfection. The equation for such an asymptote is found by setting the common denominator of Equations (18) and (19) equal to zero:

$$1 + \gamma_s S_{s,2} = 0\,, \tag{27}$$

where $S_{s,2} = (n_b + 1)^4 S_2$ and $\gamma_s = \gamma/(n_b + 1)^3$; the lowest positive solution for $\hat{M}$ of Equation (27) is the critical moment for the mth node-displacing mode. An equivalent finite-termed form of the infinite series $S_{s,2}$ is given by:

$$\begin{aligned} S_{s,2} = -\frac{1}{\sqrt{2}r_0}\Bigg[&\left(\frac{r_a r_+}{2\mu^2(1+\kappa_s)} + 1 + \hat{a}^2\right)\frac{\pi\sin\pi\sqrt{r_-/2}}{\sqrt{r_-}\left(\cos\pi\sqrt{r_-/2} - \cos\pi\eta\right)} \\ &+ \left(\frac{r_a r_-}{2\mu^2(1+\kappa_s)} - (1+\hat{a}^2)\right)\frac{\pi\sinh\pi\sqrt{r_+/2}}{\sqrt{r_+}\left(\cosh\pi\sqrt{r_+/2} - \cos\pi\eta\right)}\Bigg] \\ &+ \frac{r_a\pi^2}{2\mu^2(1+\kappa_s)\,(1-\cos\pi\eta)}\,, \end{aligned} \tag{28}$$

the derivation of which can be found in McCann (2012), where:

$$r_a = \kappa_s + 2\hat{a}\mu\sqrt{1+\kappa_s}, \tag{29}$$

$$r_0 = \sqrt{\kappa_s^2 + 4\mu^2(1+\kappa_s)}, \tag{30}$$

$$r_+ = r_0 + \kappa_s, \tag{31}$$

$$r_- = r_0 - \kappa_s, \tag{32}$$

$$\eta = m/(n_b + 1), \tag{33}$$

$$\kappa_s = \kappa/(n_b + 1)^2. \tag{34}$$

The moment factor $\mu = M/M_T$ is introduced here. The nondimensional threshold stiffness relating to the mth non-displacing mode $\gamma_{s,T,m}$ is found by setting $\mu = 1$ and solving Equation (27) for γ_s:

$$\gamma_{s,T,m} = \left[\frac{\pi^2(\kappa_s + 2\hat{a}\sqrt{1+\kappa_s})}{2(1+\kappa_s)(1-\cos\pi\eta)} + \frac{\pi\sinh\pi\sqrt{1+\kappa_s}\left(1-\hat{a}\sqrt{1+\kappa_s}\right)^2}{2(2+\kappa_s)(1+\kappa_s)^{3/2}\left(\cosh\pi\sqrt{1+\kappa_s}-\cos\pi\eta\right)}\right]^{-1}. \quad (35)$$

4.4 Mode progression

Examination of $\mathrm{d}\gamma_{s,T,m}/\mathrm{d}\eta$ provides information about the critical mode progression behavior of the system as the restraint stiffness is increased. Upon inspection, it is found that, for $a > a_{\mathrm{lim}}$, where $a_{\mathrm{lim}} = -h_s\kappa_s/4\sqrt{1+\kappa_s}$, the derivative is positive. This implies that if the restraints are positioned above a point, located $|a_{\mathrm{lim}}|$ from the shear center on the tension side of the cross-section, then, as the restraint stiffness is increased, there is a full sequential critical mode progression from $m = 1$ up to $m = n_b$, as shown in Figure 4. This is in contrast to the truncated mode progression predicted by the single harmonic representation. This, in turn, implies that the overall threshold stiffness K_T of the beam corresponds to the n_bth node-displacing mode and, when correctly rescaled, can be obtained from:

$$\gamma_{s,T} = \left[\frac{\pi^2(\kappa_s + 2\hat{a}\sqrt{1+\kappa_s})}{2(1+\kappa_s)(1+\cos\frac{\pi}{n_b+1})} + \frac{\pi\sinh\pi\sqrt{1+\kappa_s}\left(1-\hat{a}\sqrt{1+\kappa_s}\right)^2}{2(2+\kappa_s)(1+\kappa_s)^{3/2}\left(\cosh\pi\sqrt{1+\kappa_s}+\cos\frac{\pi}{n_b+1}\right)}\right]^{-1}. \quad (36)$$

When $a \leqslant a_{\mathrm{lim}}$, the derivative is not necessarily negative, but its sign now depends on the value of η. However, at a distance only slightly below a_{lim}, the derivative is negative and thus the threshold stiffness of the system is that corresponding to the first node-displacing mode *i.e.* $m = 1$. Hence it can be assumed without being overly conservative that if $a < a_{\mathrm{lim}}$ then sequential mode progression is lost, although full bracing is still achievable, as shown in Figure 5. This is in contrast to continuously-braced beams, where full bracing capability is lost for any tension side restraint (Trahair, 1979).

At a point further below a_{lim}, at a distance a_{NT} from the shear center, the moment–stiffness curve for the first node-displacing mode becomes asymptotic to the threshold moment M_T. This implies that, regardless of how stiff the restraints are, the beam cannot ever achieve full bracing, as shown in Figure 6. For $n_b = 1$, the value of $(a_{\text{lim}} - a_{\text{NT}})$ is at a maximum value of $0.048h_s$ for $\kappa_s = 0$. As $\kappa_s \to \infty$, this difference tends to $0.02h_s$. For $n_b \geqslant 2$, the difference is diminished, eventually converging to zero. Thus, it can again be assumed without being overly conservative that providing restraints at a distance greater than $|a_{\text{lim}}|$ from the shear center on the tension side of the cross-section leads to the beam not being able to achieve full bracing. As the restraint height is lowered further, the additional gain in critical moment provided by the restraint is diminished further, until when at the tension flange there is almost no increase in critical moment. The findings of this section are summarised by Figure 7. It should be noted that the curve is not asymptotic to $a = a_{\text{lim}}$; there is a finite threshold stiffness associated with this restraint height.

4.5 Comparison with "smearing" technique

Trahair (1993) detailed a method for determining the threshold stiffness and critical moment based on "smearing" the n_b discrete restraints of stiffness K into an equivalent continuous restraint of stiffness per metre $k = n_b K/L$ acting along the span of the beam. Trahair (1979) showed that single harmonic functions are legitimate solutions for the buckled shapes of continuously-restrained beams. Hence, provided the restraint stiffness is scaled appropriately, the results for critical moment and threshold stiffness obtained from the smearing technique are equivalent to those obtained by single harmonic representation of the displacement functions. Trahair commented that the smearing technique provides conservative results for the threshold stiffness of a beam with braces attached at the shear center, with the figure ranging between 1.48 and 1.91 times the actual amount for $n_b = 1$. It was then noted that the method returned more accurate values for $n_b = 2$ and it was assumed that this trend continued for higher numbers of restraints. However, when compared with the results of the current work, for $n_b \geqslant 3$, the method in fact provides threshold stiffness values that are unsafe, as shown in the example of Figure 8 for a beam with four restraints. Depending on the values of κ and a, the results can range from 0.6 to 0.9 times the actual amount. An obvious consequence of applying the smearing method is therefore the inaccurate values for the critical moment, which can often be overestimated also.

5 Validation

5.1 Critical moment

The critical moment, as calculated by the Fourier series analysis, was compared with that calculated by LTBeam (Galéa, 2003), a finite element program specialising in determining the critical moment of restrained beams. In such applications, it was reported (CTICM, 2002) that results were within 1% of those returned by more well-known finite element packages such as ABAQUS and ANSYS. A $457 \times 152 \times 82$ Universal Beam (UB) section was examined; the parameters varied and the values they assumed are outlined in Table 2. In all, for 960 separate cases, the maximum error was found to be 0.25%, with an average error of 0.06%, which can be attributed to the discretization of the beam and the inevitable rounding errors arising from this (such as the length of individual elements). This serves to validate the method of applying a full harmonic analysis to determine the elastic critical moment of a discretely-braced beam.

5.2 Deflected shape

The deflected shape of the beam was solved for by the numerical continuation software AUTO-07p (Doedel & Oldeman, 2009). The governing differential equations of the system are obtained by performing the calculus of variations (Hunt & Wadee (1998) provided an example of the procedure) on the total potential energy, V. To be suitable for use by AUTO, it is required to nondimensionalize and rescale the variables: $\tilde{u} = u/L$; $\tilde{e} = e/L$; $\tilde{\phi} = \phi$; $\tilde{x} = x/L$. The initial imperfection was $e = (L/500)\sin(\pi x/L)$. The differential equations solved by AUTO were:

$$\tilde{u}'''' - \tilde{e}'''' + \frac{ML}{EI_z}\tilde{\phi}'' + k_f\left(\frac{kL^4}{EI_z}\right)\left(\tilde{u} + \frac{a}{L}\tilde{\phi} - \tilde{e}\right) = 0, \tag{37}$$

$$\tilde{\phi}'''' + \frac{ML^3}{EI_w}\tilde{u}'' - \frac{L^2GI_t}{EI_w}\tilde{\phi}'' + ak_f\left(\frac{akL^6}{EI_w}\right)\left(\tilde{u} + \frac{a}{L}\tilde{\phi} - \tilde{e}\right) = 0, \tag{38}$$

subject to the boundary conditions $\tilde{u}(0) = \tilde{u}(1) = 0$, $\tilde{\phi}(0) = \tilde{\phi}(1) = 0$, $\tilde{u}''(0) = \tilde{u}''(1) = 0$, $\tilde{\phi}''(0) = \tilde{\phi}''(1) = 0$, where primes denote differentiation with respect to $\tilde{x}$, rather than x. In order to model the discrete restraint stiffness distribution, a piecewise-linear distribution k_f was used, with spikes possessing a base width of $2b$ and height $1/b$ centered at the restraint nodes, as shown in Figure 9. This guarantees that, upon integration, the area underneath a spike is equal to unity, as it would be if Dirac delta functions were used; these were avoided as they cause the function to be multivalued, thus leading to computational difficulties for AUTO. A value of $b = 0.01$ was decided upon; sharper distributions created problems as AUTO was sometimes unable to adapt the arclength for the continuation properly due to the size of the discretization used, leading to discontinuities in the load–deflection plots. Table 3 presents the values assumed by the parameters in the validation programme.

In all, there were 720 separate program runs, which comprised 2-parameter continuation studies with the moment being calculated at different values of the stiffness, k. For each run, a maximum of 200 points were calculated, with AUTO outputting the values of the displacement and rotation functions, which corresponded to the increasing load level. In some runs, the continuation was prematurely terminated due to the program being unable to find a convergent solution; in all, 2801 distinct observations were recorded. For each observation, the displacement functions were evaluated at 150 points along the span of the beam. In order to make a comparison with the deflected shape as calculated using the analytical methods of the current work, the coefficient of determination (R^2) was calculated to provide a quantitative measure of the goodness-of-fit between the analytical and numerical results. Tables 4 and 5 present the results of the analysis. As can be seen, the majority of the results are almost identical, indicating the accuracy of the analytical results. Figure 10 provides an appreciation of the level of goodness-of-fit implied by $R^2 > 0.999$; it can also be seen how a single harmonic function is not capable of modelling the deflected shape accurately, due to the inflection points.

6 Concluding remarks

A Rayleigh–Ritz analysis of the lateral buckling response of a beam with an arbitrary number of linearly elastic restraints located at regular intervals, positioned at an arbitrary point on its cross-section, has been successfully conducted.

Representing the DOFs as single harmonic functions can be unsafe, since a full sequential mode progression cannot be predicted. This, in turn, can lead to overestimated predictions of the value of the critical moment and creates difficulty in determining the threshold stiffness of the restraints accurately. Fourier series representations of the displacement functions leads to finite-termed closed-form solutions for the threshold stiffness and the force induced in the restraints. An implicit relationship between restraint stiffness and critical moment has also been found. An expression has been found for the limiting distance from the shear center to the position of the restraints that allows the beam to develop its full bracing capacity.

The results obtained from the full harmonic analysis of the beam were successfully validated by comparing against results obtained by two independent numerical methods. Very close agreement between the analytical and numerical results was found. Since expressions for both threshold stiffness and restraint force have been found, an approach where restraints are designed to possess both adequate stiffness and strength can be formulated.

There is scope for further development of the current work, in particular with regard to nonlinear studies into the postbuckling behavior of discretely-braced beams. The current work assumes small deflections and that the restraints can be modelled as linearly-elastic springs; with relaxation of these assumptions localizations would be expected to occur at the restraint nodes, analogous to the cellular postbuckling behavior as seen in nonlinear analyses of the stability of a strut on an elastic foundation (Hunt *et al.*, 2000) and in beams suffering from mode interaction (Wadee & Gardner, 2012).

Acknowledgements

The work was partially funded by the UK Engineering and Physical Sciences Research Council through project grant: EP/F022182/1, and also by the Department of Civil and Environmental Engineering at Imperial College London.

References

Al-Shawi, F. A. N. 2001. Stiffness of restraint for steel struts with elastic end supports. *Proceedings of the Institution of Civil Engineers - Structures and Buildings*, **146**(2), 153–159.

CTICM. 2002 (July). *LTBeam – Report on validation tests*. Tech. rept. (available with LTBeam package).

Doedel, E. J., & Oldeman, B. E. 2009. AUTO-*07p: Continuation and bifurcation software for ordinary differential equations*. Tech. rept. Department of Computer Science, Concordia University, Montreal, Canada. Available from `http://indy.cs.concordia.ca/auto`.

Flint, A. R. 1951. The influence of restraint on the stability of beams. *The Structural Engineer*, **29**(9), 235–246.

Galéa, Y. 2003. Moment critique de déversement élastique de poutre fléchies – Présentation du logiciel LTBeam. *Revue Construction Métallique – CTICM*. available to download at: www.steelbizfrance.com/telechargement/desclog.aspx?idrub=1&lng=2.

Hunt, G. W., & Wadee, M. A. 1998. Localization and mode interaction in sandwich structures. *Proceedings of the Royal Society A*, **454**, 1197–1216.

Hunt, G. W., Peletier, M. A., Champneys, A. R., Woods, P. D., Wadee, M. A., Budd, C. J., & Lord, G. J. 2000. Cellular buckling in long structures. *Nonlinear Dynamics*, **21**(1), 3–29.

McCann, F. 2012. *Stability of beams with discrete lateral restraints*. Ph.D. thesis, Imperial College London.

Medland, I. C. 1980. Buckling of interbraced beam systems. *Engineering Structures*, **2**(2), 90–96.

Mutton, B. R., & Trahair, N. S. 1973. Stiffness requirements for lateral bracing. *Journal of the Structural Division, ASCE*, **99**(10), 2167–2182.

Nethercot, D. A., & Rockey, K. C. 1971. Finite element solutions for the buckling of columns and beams. *International Journal of Mechanical Sciences*, **13**(11), 945–949.

Pi, Y. L., Trahair, N. S., & Rajasekaran, S. 1992. Energy equation for beam lateral buckling. *Journal of Structural Engineering, ASCE*, **118**(6), 1462–1479.

Steel Construction Institute. 2009. *Steel building design: Design data – in accordance with Eurocodes and the UK National Annexes.* Ascot, UK: Steel Construction Institute. SCI Publication P363.

Taylor, A. C., & Ojalvo, M. 1966. Torsional restraint of lateral buckling. *Journal of the Structural Division, ASCE*, **92**(2), 115–129.

Thompson, J. M. T., & Hunt, G. W. 1984. *Elastic instability phenomena.* New York: John Wiley and Sons.

Timoshenko, S. P., & Gere, J. M. 1961. *Theory of elastic stability.* 2nd edn. New York: McGraw-Hill.

Trahair, N. S. 1979. Elastic lateral buckling of continuously restrained beam columns. *Pages 61–73 of:* Campbell-Allen, D., & Davis, E. H. (eds), *The Profession of a Civil Engineer.* Sydney University Press.

Trahair, N. S., & Nethercot, D. A. 1984. Bracing requirements in thin-walled structures. *Chap. 3, pages 93–130 of:* Rhodes, J., & Walker, A. C. (eds), *Developments in Thin-Walled Structures Volume 2.* London: Elsevier Applied Science Publishers.

Trahair, N. S., Bradford, M. A., Nethercot, D. A., & Gardner, L. 2008. *The Behaviour and Design of Steel Structures to EC3.* 4th edn. London: Taylor and Francis.

Trahair, N.S. 1993. *Flexural-torsional buckling of structures.* London: E & FN SPON.

Vlasov, V. Z. 1961. *Thin-walled elastic beams.* 2nd edn. Jerusalem, Israel: Israel Program for Scientific Translations.

Wadee, M. A., & Gardner, L. 2012. Cellular buckling from mode interaction in I-beams under uniform bending. *Proceedings of the Royal Society A*, **468**(2137), 245–268.

Winter, G. 1960. Lateral bracing of columns and beams. *ASCE Transactions*, **125**, 807–826.

Yura, J. A. 2001. Fundamentals of beam bracing. *Engineering Journal, American Institute of Steel Construction*, **38**(1), 11–26.

Zuk, W. 1956. Lateral bracing forces on beams and columns. *Journal of the Engineering Mechanics Division, ASCE*, **82**(3), 1032–1 – 1032–16.

Figure Captions

Figure 1: Cross-sectional geometry, system axes and configuration of the model.

Figure 2: Typical critical mode progression for beams with discrete restraints when assuming single harmonic functions for the displacement functions.

Figure 3: Demonstration of mode-skipping for a beam with five discrete restraints ($\hat{a} = 0.5$, $\kappa = 5$).

Figure 4: Typical moment–stiffness curves demonstrating sequential critical mode progression ($n_b = 3$, $\hat{a} = 0.5$, $\kappa_s = 0.5$).

Figure 5: Typical moment–stiffness curves demonstrating the loss of sequential critical mode progression for $a < a_{\text{lim}}$ ($n_b = 3$, $\hat{a} = -0.225$, $\kappa_s = 0.5$).

Figure 6: Typical moment–stiffness curves demonstrating the loss of full bracing capability for $a < a_{NT}$ ($n_b = 3$, $\hat{a} = -0.25$, $\kappa_s = 0.5$).

Figure 7: The effect of restraint height on bracing ability.

Figure 8: Moment–stiffness curves for a beam with four restraints ($\hat{a} = 0.5$, $\kappa_s = 0.5$), demonstrating how the "smearing" method can predict underestimated, and hence unsafe, threshold stiffness values, as well as overestimated strength values.

Figure 9: The piecewise stiffness distribution function for a beam with three restraints, and a restraint width of $L/50$ ($b = 0.01$).

Figure 10: Typical graph of u/L against x/L for $R^2 > 0.999$ (this example: $L = 7$ m, $\hat{a} = 0$, $n_b = 5$, $M/M_T = 0.676$ and $K/K_T = 0.5$).

$457 \times 152 \times 82$	
h_s	446.9 mm
I_z	1185 cm^4
I_w	0.591 dm^6
I_t	89.2 cm^4

Table 1: Relevant section properties of $457 \times 152 \times 82$ UB section.

Parameter	Values assumed
n_b	1, 2, 3, 4, 5, 6
$\hat{a}$	$\hat{a}_{\text{lim}}$, 0, 0.5, 1
L (m)	7, 8.75, 10.5, 12.25, 14

Table 2: Values assumed for the parameters in the validation using LTBeam.

Parameter	Values assumed
n_b	1, 2, 3, 4, 5, 6
$\hat{a}$	0, 0.5, 1
L (m)	7, 8.75, 10.5, 12.25, 14

Table 3: Values assumed by the parameters in the validation using AUTO.

Value of R^2	Observations	Percentage of total
> 0.999	1936	69.1
$0.99 - 0.999$	446	15.9
$0.98 - 0.99$	81	2.9
$0.96 - 0.98$	64	2.3
$0.90 - 0.96$	70	2.5
< 0.90	204	7.3

Table 4: Distribution of the coefficient of determination (R^2) values between the analytical and AUTO results for the lateral deflection, u.

Value of R^2	Observations	Percentage of total
> 0.999	2020	72.1
$0.99 - 0.999$	392	14.0
$0.98 - 0.99$	66	2.4
$0.96 - 0.98$	69	2.5
$0.90 - 0.96$	73	2.6
< 0.90	181	6.5

Table 5: Distribution of the coefficient of determination (R^2) values between the analytical and AUTO results for the angle of twist, ϕ.

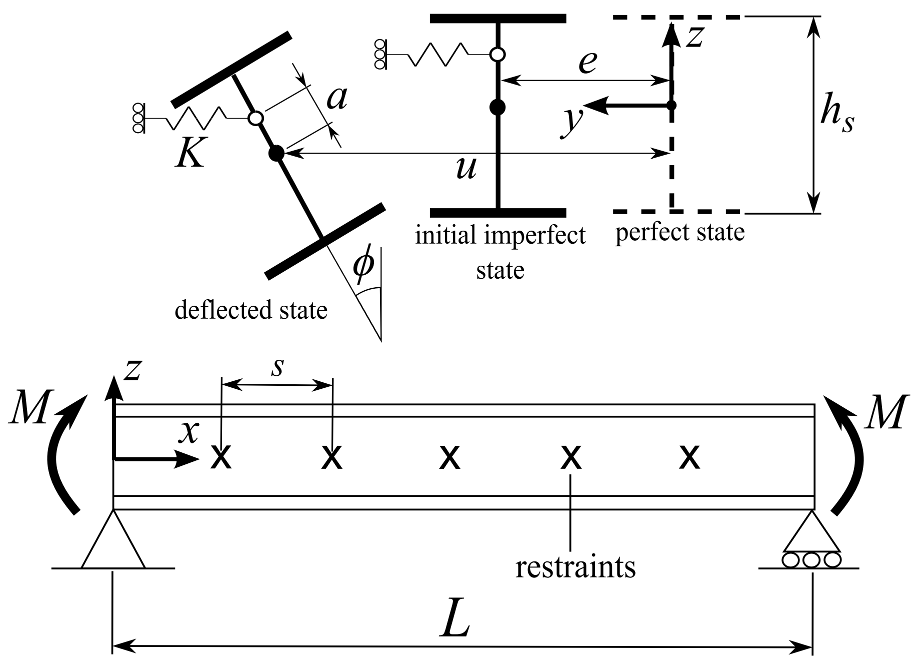

Figure 1: Cross-sectional geometry, system axes and configuration of the model.

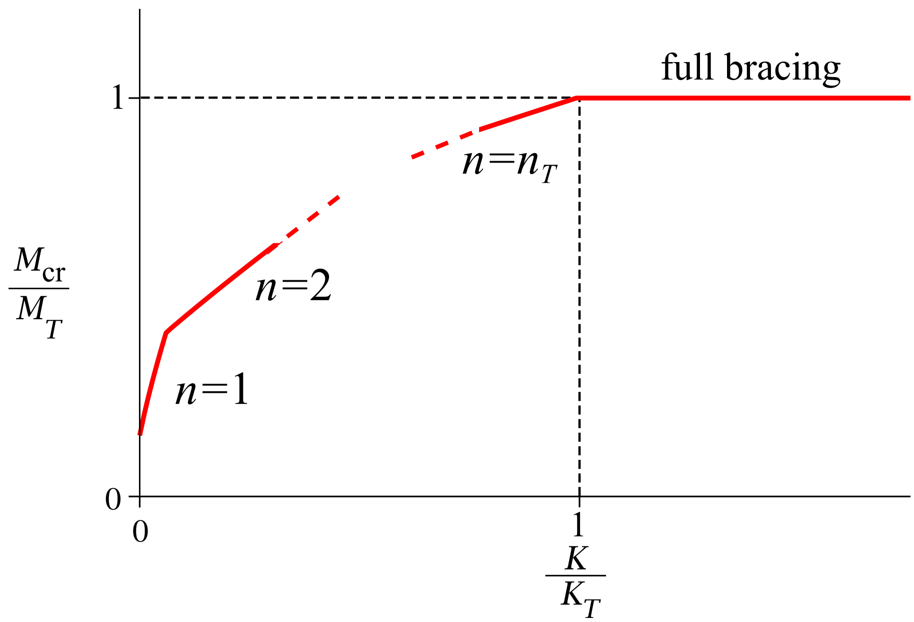

Figure 2: Typical critical mode progression for beams with discrete restraints when assuming single harmonic functions for the displacement functions.

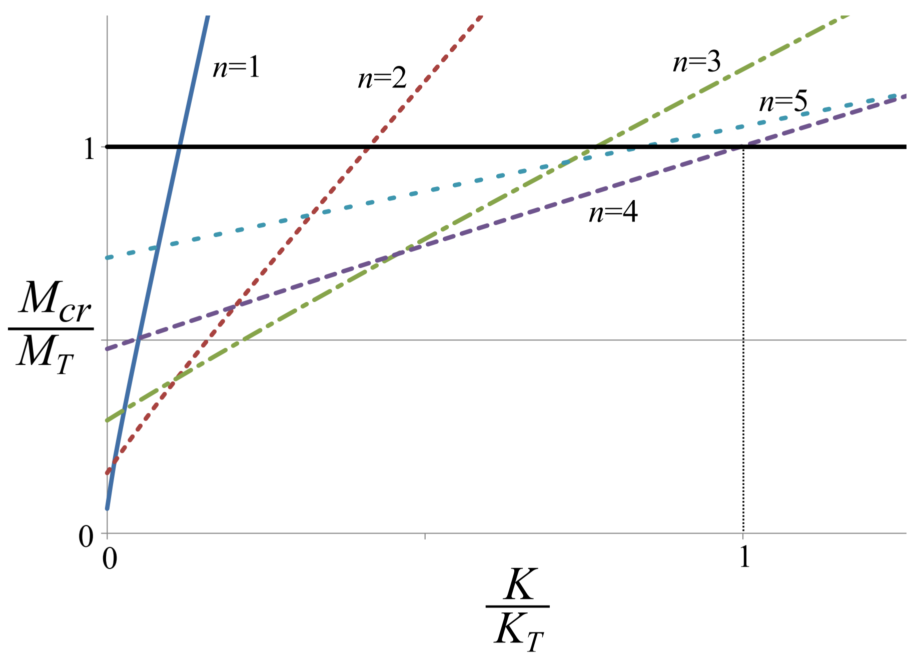

Figure 3: Demonstration of mode-skipping for a beam with five discrete restraints ($\hat{a} = 0.5$, $\kappa = 5$).

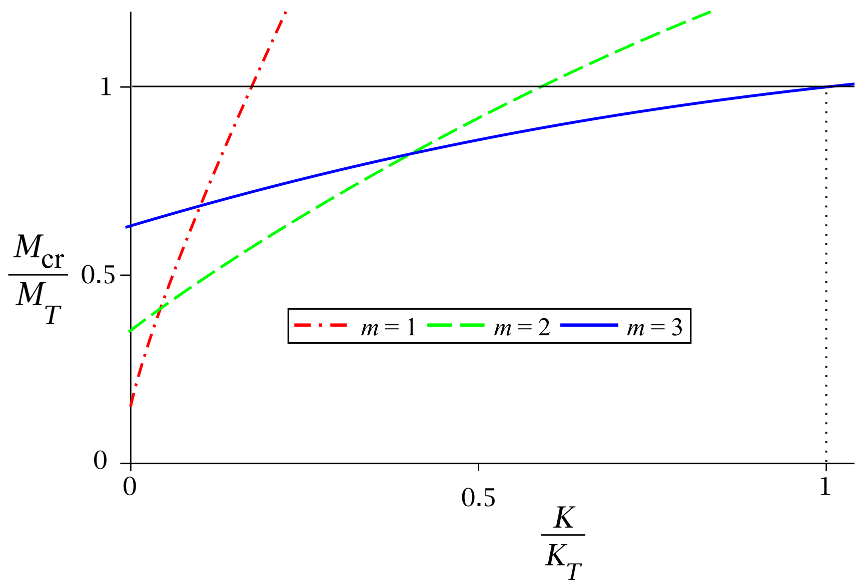

Figure 4: Typical moment–stiffness curves demonstrating sequential critical mode progression ($n_b = 3$, $\hat{a} = 0.5$, $\kappa_s = 0.5$).

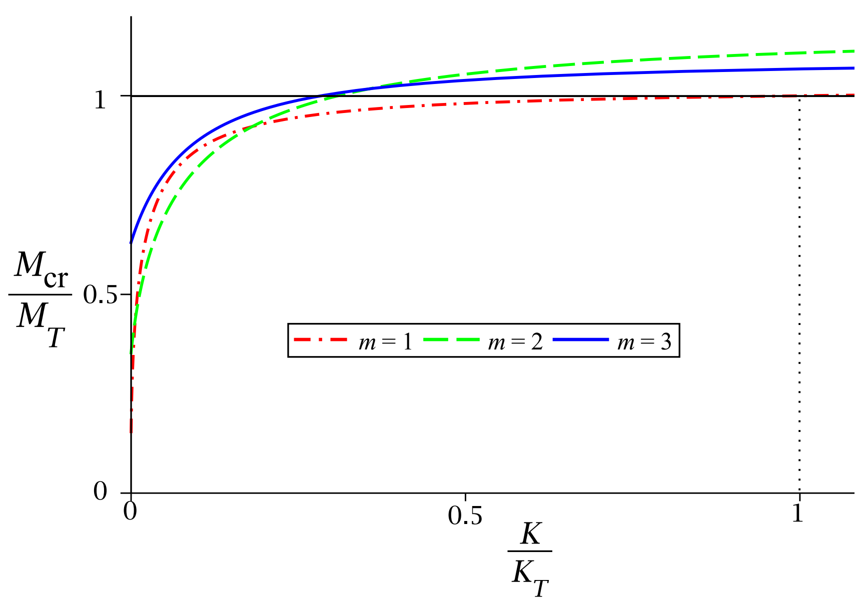

Figure 5: Typical moment–stiffness curves demonstrating the loss of sequential critical mode progression for $a < a_{\lim}$ ($n_b = 3$, $\hat{a} = -0.225$, $\kappa_s = 0.5$).

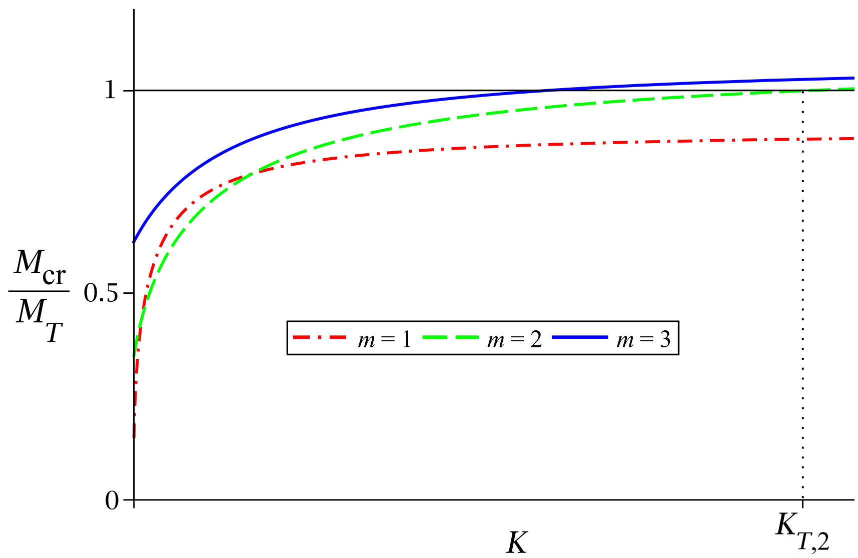

Figure 6: Typical moment–stiffness curves demonstrating the loss of full bracing capability for $a < a_{NT}$ ($n_b = 3$, $\hat{a} = -0.25$, $\kappa_s = 0.5$).

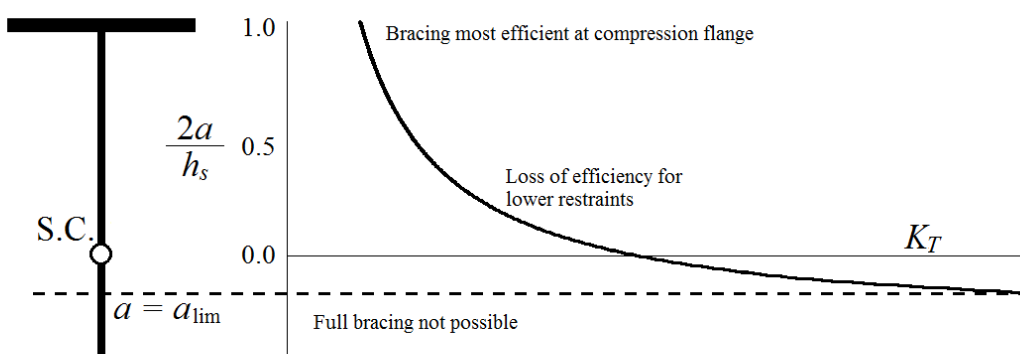

Figure 7: The effect of restraint height on bracing ability.

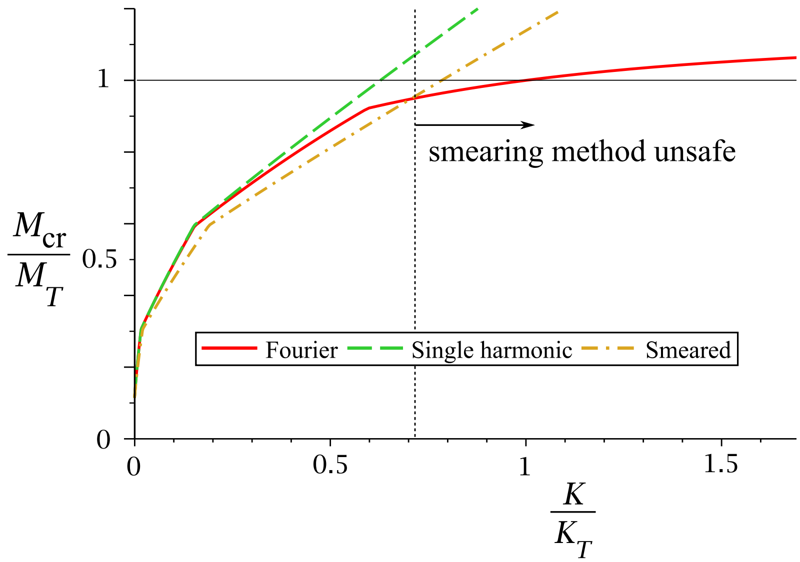

Figure 8: Moment–stiffness curves for a beam with four restraints ($\hat{a} = 0.5$, $\kappa_s = 0.5$), demonstrating how the "smearing" method can predict underestimated, and hence unsafe, threshold stiffness values, as well as overestimated strength values.

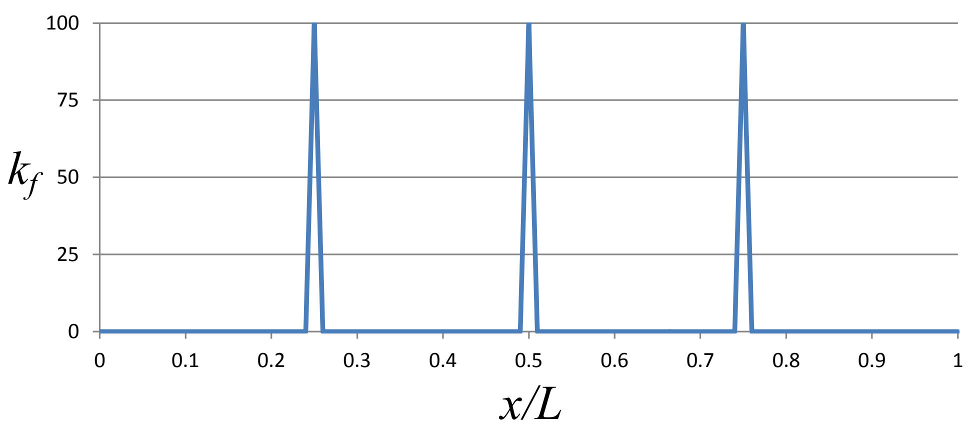

Figure 9: The piecewise stiffness distribution function for a beam with three restraints, and a restraint width of $L/50$ ($b = 0.01$).

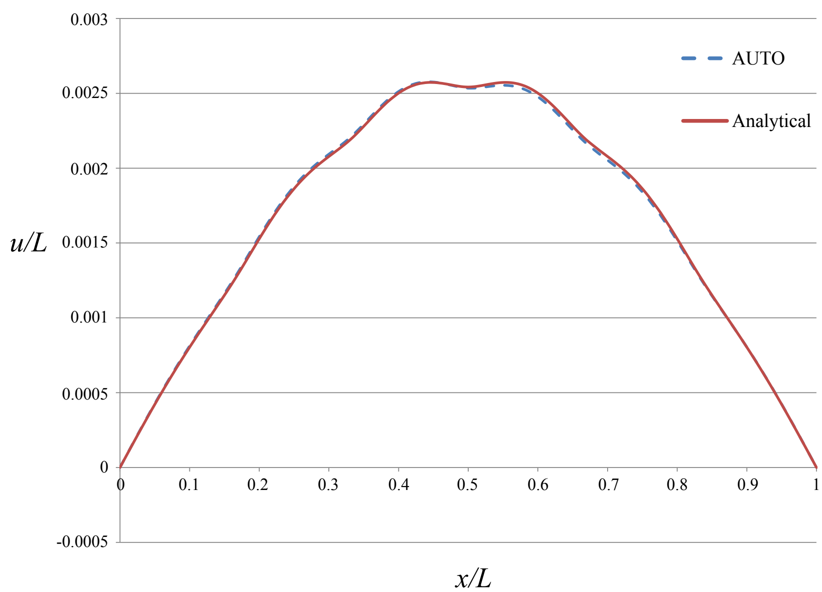

Figure 10: Typical graph of u/L against x/L for $R^2 > 0.999$ (this example: $L = 7$ m, $\hat{a} = 0$, $n_b = 5$, $M/M_T = 0.676$ and $K/K_T = 0.5$).